Measures of chaos and equipartition in integrable and nonintegrable lattices

Norman J. Zabusky,[a] Zhanyu Sun, and Gaozhu Peng
Department of Mechanical and Aerospace Engineering and CAIP Center, Rutgers University, Piscataway, New Jersey 08855

(Received 18 August 2005; accepted 16 December 2005; published online 30 March 2006)

We have simulated numerically the behavior of the one-dimensional, periodic FPU-alpha and Toda lattices to optical and acoustic initial excitations of small-but finite and large amplitudes. For the small-through-intermediate amplitudes (small initial energy per particle) we find nearly recurrent solutions, where the acoustic result is due to the appearance of solitons and where the optical result is due to the appearance of localized breather-like packets. For large amplitudes, we find complex-but-regular behavior for the Toda lattice and "stochastic" or chaotic behaviors for the alpha lattice. We have *used the well-known diagnostics: Localization parameter; Lyapounov exponent*, and *slope of a linear fit to linear normal mode energy spectra*. Space-time diagrams of *local particle energy* and a *wave-related* quantity, a discretized Riemann invariant are also shown. The discretized Riemann invariants of the alpha lattice reveal soliton and near-soliton properties for acoustic excitations. Except for the localization parameter, there is a clear separation in behaviors at long-time between integrable and nonintegrable systems. © *2006 American Institute of Physics*.
[DOI: 10.1063/1.2165592]

To quantify the appearance of chaos in nonlinear Hamiltonian lattice dynamics numerical experiments, we examine the properties of the: Maximum Lyapounov exponents, energy spectra, and a shifted-discretized Riemann invariant (a wave-related quantity). At a time decreasing with an increasing average initial energy particle, we find a clear separation in behavior of these quantifiers when we compare simulations of the nonintegrable FPU alpha and integrable Toda lattices. The former always shows the approach to equipartition at long times.

INTRODUCTION

In this paper we explore the route to energy equipartition or *thermalization* in a nonintegrable Hamiltonian lattice, the alpha FPU lattice [Fermi, Pasta, and Ulam (1955)], by comparing the transient dynamics with the integrable Toda lattice (Toda, 1967a; 1967b; 1969; 1981), which does *not* show energy equipartition. We use both acoustic (long wavelength) and zone-boundary mode (short wavelength) initial conditions at several levels of excitation. Many valuable papers on this subject have recently been presented in the Chaos Focus issue (Vol. 15) on the FPU problem. Of particular interest to the present paper is the work of Berman and Izrailev (2005), Dauxois *et al.* (2005), Pettini *et al.* (2005), and Zabusky (2005).

The primary goal of our paper is to compare the performance of several diagnostics that bear on chaotic evolutions that may result in equipartition of energy among the modes of the system. The secondary goal is to present a *new near-recurrence* for the alpha and Toda lattices when excited initially by a localized optical excitation at low-to-intermediate energies.

We examine the sharing of energy equally among all the linear modal energies by calculating the slope of the line fitted to *all* the linear modal energies; the maximum Lyapounov exponent and a localization factor for physical space energy density. For the acoustic mode, we also use a *discretized Riemann invariant* as proposed in Zabusky (1968). This diagnostic reveals the coupling during the interaction of soliton-like pulses traveling along both left- and right-propagating characteristic directions. We present visualizations with space-time diagrams of local energy and graphs of local energy and other revealing diagnostics. The details of the largest Lyapounov exponent diagnostic are given in the Appendix.

After Fermi-Pasta-Ulam, Zabusky and Deem were the first to experiment systematically with the FPU alpha lattice. Deem, Zabusky, and Kruskal (1965) produced a sequence of computer generated animations, including simulations of the alpha-lattice and the Korteweg-de Vries (KdV) equation (pde). With *periodic* boundaries and a single long-wavelength-*propagating-mode* initial condition, they observed near-recurrence for both the lattice and the pde (Zabusky, 1969). Tuck and Menzel (1972) initialized a lowest mode with fixed boundary conditions and found a super near-recurrence after 14 near recurrences. Izrailev and Chirikov (1966), for the beta lattice, presented an analytically derived scaling law using the resonance-overlap idea. They derived a transition boundary between regular and chaotic evolution at high and low wave numbers of the initial excitation. Zabusky and Deem (1967) claimed to have found near-equipartition in a very short time calculation. They used an initial Gaussian-modulated localized optical excitation

[a]Author to whom correspondence should be addressed. Telephone: 732-445-5869. Electronic mail: nzabusky@caip.rutgers.edu

[i.e., one that has a Gaussian envelope in physical space and modulates the highest zone boundary (or π-) mode]. By modern computational standards, all these simulations were done for *short* times, and did not reveal the systematic transition to strong chaos and equipartition, as discussed below.

Equipartition for the FPU-alpha lattice with finite N was first illustrated numerically by Bochieri *et al.* (1970). In carefully executed numerical work Casetti *et al.* (1997) focused on Lyapounov exponents for the alpha and Toda lattices and Shelepansky (1997) examined low energy chaos for the alpha lattice [see also Dauxois *et al.* (1997) and Dauxois *et al.* (1998)]. Rink's (2001) mathematical work focused on the periodic FPU lattice, in particular the beta lattice. Rink (2005) remarks, "…[the alpha lattice] does not always seem integrable or near-integrable as opposed to the beta lattice which has a full set of near integrals." (Note, one must examine his work carefully and consider how he uses the term "near-integrable.") Recently, Chechin *et al.* (2002, 2004) have identified groups or "bushes" of normal modes (or fixed point sets of the natural discrete symmetries) of the FPU alpha and beta lattices, which are automatically invariant manifolds. They applied Floquet methods to study the stability of these bushes in one and two dimensions. For the one-dimensional (1D) alpha lattice some bushes are stable at low energy. The initial conditions in the present paper are not in the special classes of these bushes. Thus, for any amplitude of excitation, one expects eventual equipartition among all the modes.

EQUATIONS OF MOTION AND INITIAL CONDITIONS

The equations solved were

$$\omega_o^{-2}\ddot{y}_j = (y_{j+1} - 2y_j + y_{j-1})[1 + \alpha(y_{j+1} - y_{j-1})], \tag{1a}$$

$$\omega_o^{-2}\ddot{y}_j = -\frac{1}{2\alpha}[e^{2\alpha(y_j - y_{j+1})} + e^{2\alpha(y_{j-1} - y_j)}], \tag{1b}$$

the α-lattice and the Toda lattice, respectively. The boundary conditions were periodic over an interval of 2N coupled masses. The "optical" or highest linear frequency of the lattice is $2\omega_o$. In our simulations we assume $\alpha = \omega_o = 1$ and vary the initial conditions by changing the amplitude of the initial excitation. Note, because of the signs chosen in (1a) and (1b), the Toda lattice with $\alpha = 1$ corresponds to the alpha lattice with $\alpha = -1$.

For the acoustic initial conditions we chose a lowest mode in the periodic domain. Here $y_j(0) = a \sin(j\pi/N)$ and $\dot{y}_j(0)$ was computed from the discretized Riemann invariant [as discussed below in Eq. (13a)], so as to obtain a positive propagating wave at low energies. For the optical initial condition, we chose a localized Gaussian-modulated

$$y_j(0) = (-1)^j \eta \exp\left[-\left(\frac{j-N}{\Delta N}\right)^2\right], \quad \dot{y}_j(0) = 0,$$
$$j = 1, 2, \ldots, 2N. \tag{2}$$

The Yoshida sixth-order symplectic integrator [Yoshida (1990)] was used with a time step of 0.01, or 628 time steps for the period corresponding to the highest linear frequency of the lattice. The floating point numbers were double precision. To validate the computational code, we ran the alpha lattice with the optical I.C. ($\eta = 0.188$, $\alpha = 1$, $\Delta = 0.1$, $N = 600$) forward to $t = 3000$ (300 000 steps) to obtain $y_n(3,000)$ *and* $\dot{y}_n(3,000)$. With this precise data, we set the time interval to a corresponding negative value and computed to 3000 to obtain $y_n^*(0)$ *and* $\dot{y}_n^*(0)$. Figures 1(a) and 1(b) show that $\dot{y}_n^*(0)$ and $y_n^*(0) - y_n(0)$, have very small magnitudes. In particular $\max|\dot{y}_n^*(0)| \sim 2 \times 10^{-12}$ and $\Sigma_1^{2N}\dot{y}_n^*(0) = 5.69 \times 10^{-16}$. The average displacement is negative, $\Sigma_1^{2N} y_n(0) = -7.69 \times 10^{-11}$, $\Sigma_1^{2N} y_n^*(0) = -2.59 \times 10^{-11}$. These very small errors of the Yoshida sixth-order symplectic integrator indicate that it can perform long-time calculations with high accuracy.

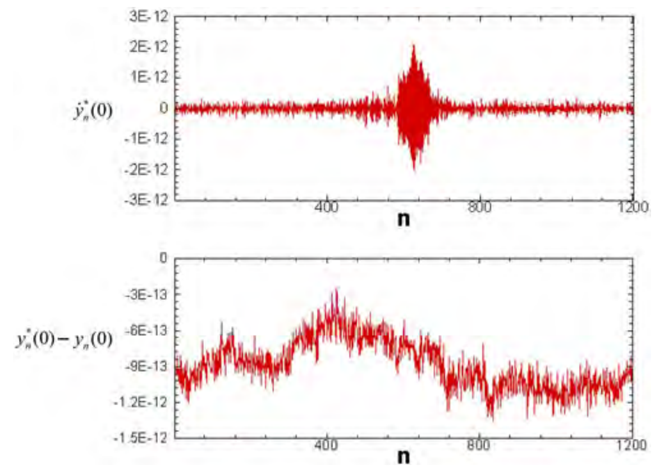

FIG. 1. The result of computing to $t = 3000$ and reversing time and computing back to zero. (a) $\dot{y}_n^*(0)$, (b) $y_n^*(0) - y_n(0)$.

WAVE AND OSCILLATION PHENOMENA

Continuum limits

For acoustic and optical *small-amplitude* initial excitations all phenomena to long times may be obtained from two variables. We rederive the Zabusky-Deem (1967) coupled partial differential equations to facilitate a better understanding of the observed phenomena presented below. For all initial excitations, we assume that the time step of the numerical simulations is sufficiently small and the integrator sufficiently accurate so that temporal discretization errors may be neglected.

First we label the odd and even masses, $w_n \equiv y_{2n+1}$ *and* $z_n \equiv y_{2n}$ and rewrite the single discrete equation (1a) as two coupled equations. Next we expand w and z in a power series in space, e.g., for w

$$w_{n\pm1} = w \pm h\partial_x w + \frac{h^2}{2}\partial_x^2 w \pm \frac{h^3}{3!}\partial_x^3 w + \cdots,$$

and substitute in these equations and then add and subtract them. We introduce

$$u(x,t) = \frac{w(x,t) + z(x,t)}{2}, \tag{3}$$

$$v(x,t) = \frac{w(x,t) - z(x,t)}{2}, \tag{4}$$

and obtain a coupled set of equations. For u

$$\begin{aligned} c_A^{-2}\partial_t^2 u &= \partial_x^2 u + \frac{h^2}{4!}\partial_x^4 u + \frac{h^4}{6!}\partial_x^6 u + 4\varepsilon v \partial_x\left(v + \frac{h^2}{3!}\partial_x^2 v \right.\\ &\quad \left. + \frac{h^4}{5!}\partial_x^4 v\right) + 2\varepsilon\left\{ \partial_x u\left[h^2\partial_x^2 u + \frac{h^4}{4!}\partial_x^4 u + \frac{h^6}{6!}\partial_x^6 u\right]\right.\\ &\quad \left. + \frac{h^2}{3!}\partial_x^3 u\left[h^2\partial_x^2 u + \frac{h^4}{4!}\partial_x^4 u\right] + \frac{h^4}{5!}\partial_x^5 u[h^2\partial_x^2 u]\right.\\ &\quad + 2\varepsilon\left\{ \partial_x v\left[h^2\partial_x^2 v + \frac{h^4}{4!}\partial_x^4 v + \frac{h^6}{6!}\partial_x^6 v\right]\right.\\ &\quad \left. + \frac{h^2}{3!}\partial_x^3 v\left[h^2\partial_x^2 v + \frac{h^4}{4!}\partial_x^4 v\right] + \frac{h^4}{5!}\partial_x^5 v[h^2\partial_x^2 v]\right.\\ &\quad + O(h^6) + O(\varepsilon h^6), \end{aligned} \tag{5}$$

and a comparable equation for v. Here, $c_A = h\omega_o$ is the acoustic speed and two small parameters, ε *and* h, where $\varepsilon = 2\alpha h$ and $h = \mathrm{L}/\mathrm{N}$ is the length interval between the masses. If higher-order terms are omitted, we obtain the equations introduced by Zabusky and Deem (1967)

$$\begin{aligned} c_A^{-2}\partial_t^2 u &= \partial_x^2 u + \frac{h^2}{12}\partial_x^4 u + 4\varepsilon v \partial_x\left(v + \frac{1}{6}\partial_x^2 v\right)\\ &\quad + \frac{\varepsilon}{2}\partial_x[(\partial_x u)^2 + (\partial_x v)^2] + O(\varepsilon h^2) + O(h^2), \end{aligned} \tag{6a}$$

$$\begin{aligned} \omega_o^{-2}\partial_t^2 v &= -4v - h^2\partial_x^2 v - \frac{h^4}{12}\partial_x^4 v - 4\varepsilon v \partial_x\left(u + \frac{h^2}{6}\partial_x^2 u\right)\\ &\quad - \frac{\varepsilon h^2}{2}\partial_x[(\partial_x u)(\partial_x v)] + O(\varepsilon h^2) + O(h^2), \end{aligned} \tag{6b}$$

where $u(x,t)$ corresponds to the acoustical region and $v(x,t)$ corresponds to the optical or zone-boundary region. Thus, if $O(\varepsilon h^4) = 0$ and $h^4 \ll 1$ and $\varepsilon \ll 1$: The *u-phenomena* (acoustic motions) are described by a dispersively modified nonlinear hyperbolic equation which is forced by even (quadratic) terms of v. The *v-phenomena* (optical oscillations) are described by a dispersively modified oscillator equation which is forced by products of odd terms in v and u. The dispersive-modification of the latter causes the energy to "spread " from its initial compact location and finally result in a configuration which is modulationally unstable. An array of *localized high frequency packets (possibly discrete breathers)*, emerge and interact. At low to intermediate energies we see a new near-recurrent behavior for both alpha and Toda lattices, as described below.

First, let us discuss several simple continuum models. For initial long wavelength small-but-finite acoustic excitations, we set $v = 0$. Since the nonlinear terms provide the primary source of energy coupling among the modes which can lead to chaos, we first focus on the dispersionless equation obtained by omitting terms $O(h^2)$ in (6a), and obtain the nonlinear hyperbolic pde

$$c_A^{-2}\partial_t^2 u - (1 + \varepsilon\partial_x u)\partial_x^2 u = 0. \tag{7}$$

This can be written as the coupled set of first-order Riemann invariant equations

$$c_A^{-1}\partial_t r_\pm = \mp [1 + (3\varepsilon/2)(r_+ + r_-)]^{1/3}(\partial_x r_\pm) = 0 \tag{8a}$$

or

$$c_A^{-1}\partial_t r_\pm = \mp [1 + (\varepsilon/2)(r_+ + r_-)](\partial_x r_\pm) + O(\varepsilon^2), \tag{8b}$$

where

$$r_\pm = \left(\tfrac{1}{2}\right)\{\pm c_A^{-1}\partial_t u + (2/3\varepsilon)[(1 + \varepsilon\partial_x u)^{3/2} - 1]\}, \tag{9a}$$

or

$$\partial_x u = \varepsilon^{-1}\left[1 + \frac{3\varepsilon}{2}(r_+ + r_-)\right]^{2/3} - 1, \tag{9b}$$

and

$$c_A^{-1}\partial_t u = (r_+ - r_-). \tag{9c}$$

Zabusky (1962) and Kruskal and Zabusky (1964) first showed that a singularity in $\partial_x u$ develops in a finite time. Thus, if we include the next, fourth derivative, dispersive term from the u equation and expand in a power series, then Eq. (8b) generalizes to

$$\begin{aligned} c_A^{-1}\partial_t r_\pm &= \mp [1 + (\varepsilon/2)(r_+ + r_-)](\partial_x r_\pm)\\ &\quad \mp (h^2/24)\partial_{xxx}(r_+ + r_-) + O(\varepsilon^2) + O(\varepsilon h^2) + O(h^4). \end{aligned} \tag{10}$$

If we choose an initial condition such that $r_+(x,0) = 0$, and assume a weak nonlinear process, we may omit the evolution of $r_+(x,t)$ and so obtain

$$\partial_{t^*}\tilde{r} = (\varepsilon/2)\tilde{r}(\partial_{x^*}\tilde{r}) + (h^2/24)(\partial_{x^*x^*x^*}\tilde{r}), \tag{11}$$

where $t^* = c_A t, x^* = x - c_A t$, and $\tilde{r} = r(x^*, t^*)$. This is the integrable Korteweg deVries equation, which describes, in a "shifted" reference frame, the evolution of weak nonlinear phenomena on the alpha and Toda lattices for long times, as discussed below.

ACOUSTIC EXCITATIONS

In the mid and late 60's, Zabusky, Kruskal, and Deem, motivated by their solutions of the Korteweg-de Vries (KdV) equation on a *periodic* domain (Deem, Zabusky, and Kruskal, 1965; Zabusky and Kruskal, 1965), used a periodic alpha-lattice and also found near recurrences (Zabusky, 1969; Zabusky, 1981).

The time derivative of the acoustic I.C. was obtained by first discretizing the *Riemann invariant* (9a) with

$$\begin{aligned} \tilde{r}_\pm(n,t) &= \tfrac{1}{2}\Big\{\pm(N/\omega_o)\partial_t y_n\\ &\quad + \tfrac{1}{3}(N/\alpha)[(1 + 2\alpha(y_{n+1} - y_n))^{3/2} - 1]\Big\},\\ &\quad (1 \le n \le 2N). \end{aligned} \tag{12}$$

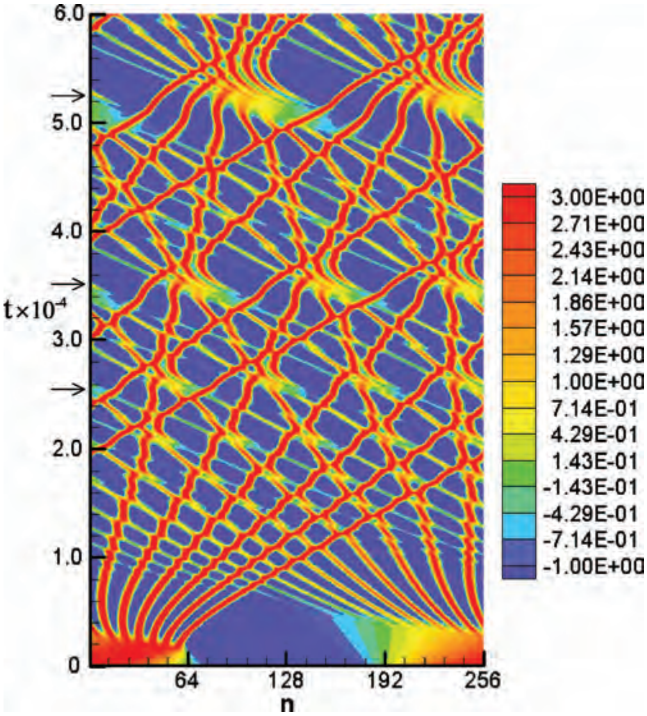

FIG. 2. (Color) S-t diagram of shifted-$r_-(n,t)$ for α lattice with the acoustic I.C. ($\alpha=1$ and $a=1, \varepsilon=3.01\times10^{-4}$) up to $t=60\,000$. The three arrows from bottom to top point out $\frac{1}{4}T_R$, $\frac{1}{3}T_R$, and $\frac{1}{2}T_R$, respectively.

Note, we have used a simple forward difference for the first space derivative. For ease, we set $y_n(0)=a\sin(n\pi/N)$, $(1 \leqslant n \leqslant 2N)$, and $\tilde{r}_+(n,0)=0$, then

$$\dot{y}_n(0)=\frac{1}{3}(\omega_o/\alpha)[1-(1+2\alpha(y_{n+1}-y_n))^{3/2}], \tag{13a}$$

or

TABLE I. Parameters for acoustic (Ac.) and optical (Opt.) simulations for lattice of length 2N. Here $\varepsilon=(\text{Total energy})/2N$.

Lattice	I.C.	Δ	$10^4\varepsilon$	a or η	Total energy	N
α	Ac.	NA	3.01	1	0.077	128
α	Opt.	0.1	28.2	0.15	0.720	128
Toda	Opt.	0.1	28.2	0.148 456	0.720	128
α	Ac.	NA	28.2	3.057 84	0.720	128
Toda	Ac.	NA	28.2	3.056 764	0.720	128
α	Opt.	0.1	5.63	0.212 132	1.441	128
Toda	Opt.	0.1	5.63	0.207 874	1.441	128
α	Ac.	NA	5.63	4.327 82	1.441	128
Toda	Ac.	NA	5.63	6.097 945	1.441	128
α	Opt.	0.1	113	0.3	2.883	128
Toda	Opt.	0.1	113	0.288 524	2.883	128
α	Ac.	NA	113	6.117 34	2.883	128
Toda	Ac.	NA	113	6.108 73	2.883	128
α	Opt.	0.1	0.501	0.020	0.020	200
α	Opt.	0.1	4.51	0.180	0.180	200
α	Opt.	0.1	33.3	1.33	1.33	200
α	Opt.	0.1	133	5.32	5.32	200
α	Opt.	0.1	443	5.32	5.32	600

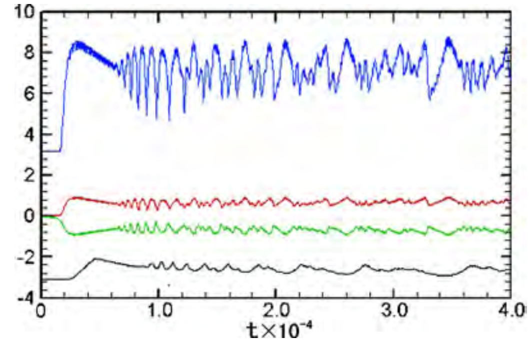

FIG. 3. The maximum and minimum of r_+ and r_- vs time for α lattice with the acoustic I.C. of Fig. 1 ($\alpha=1$, $a=1, \varepsilon=3.01\times10^{-4}$) up to $t=40\,000$. From top to bottom shows max(r_-), max(r_+), min(r_+), and min(r_-), respectively.

$$r_-(n,0)=\frac{1}{3}(N/\alpha)[(1+2\alpha(y_{n+1}-y_n))^{3/2}-1]$$

$$=a\pi\cos\left(\pi\left(n+\frac{1}{2}\right)\right)$$

$$-\frac{(\pi a)^2}{8N}\left[\cos\left(2\pi\left(n+\frac{1}{2}\right)\right)-\right]+O(N^{-2}). \tag{13b}$$

In (13b) and below we *suppress the tilde*, previously used to designate the discretized invariant. In the work below, the identical initial conditions are used for the Toda lattice, despite the fact that they are not the corresponding Riemann invariants for the continuum of the Toda lattice. To make the appearances of the r_- s-t diagrams similar to KdV s-t diagrams, we plotted the results in a Galilean frame moving to the right with c_A, the linear acoustic speed. That is, on the *shifted* s-t diagram the characteristic of a right-going linear acoustic wave would be a vertical line.

A sample result of the *shifted*-r_- (n,t) s-t diagram is shown in Fig. 2 for $2N=256$, $\alpha=1$, $a=1$, and $\varepsilon=3.01\times10^{-4}$. (See Table I for the parameters used for all runs in this paper.) We now describe the phenomena that was first observed by Zabusky and Kruskal (1965) for the KdV equation: At early times, one sees characteristics converging in space at $N=64$ at the "breakdown" time $t_B=1800$; emerging immediately and moving to the right at the highest speed is the strongest acoustic "near-soliton;" at about 7000 it col-

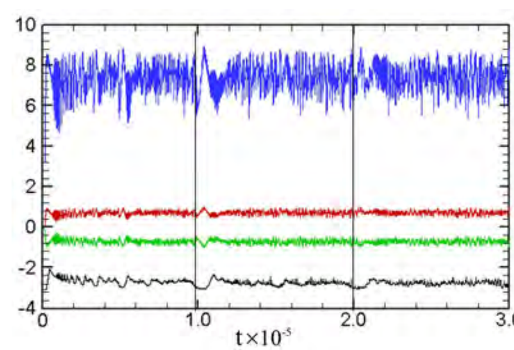

FIG. 4. The maximum and minimum of r_+ and r_- vs time for α lattice with the acoustic I.C. ($\alpha=1$, and $a=1, \varepsilon=3.01\times10^{-4}$) up to $t=300\,000$. From top to bottom shows max(r_-), max(r_+), min(r_+), and min(r_-), respectively.

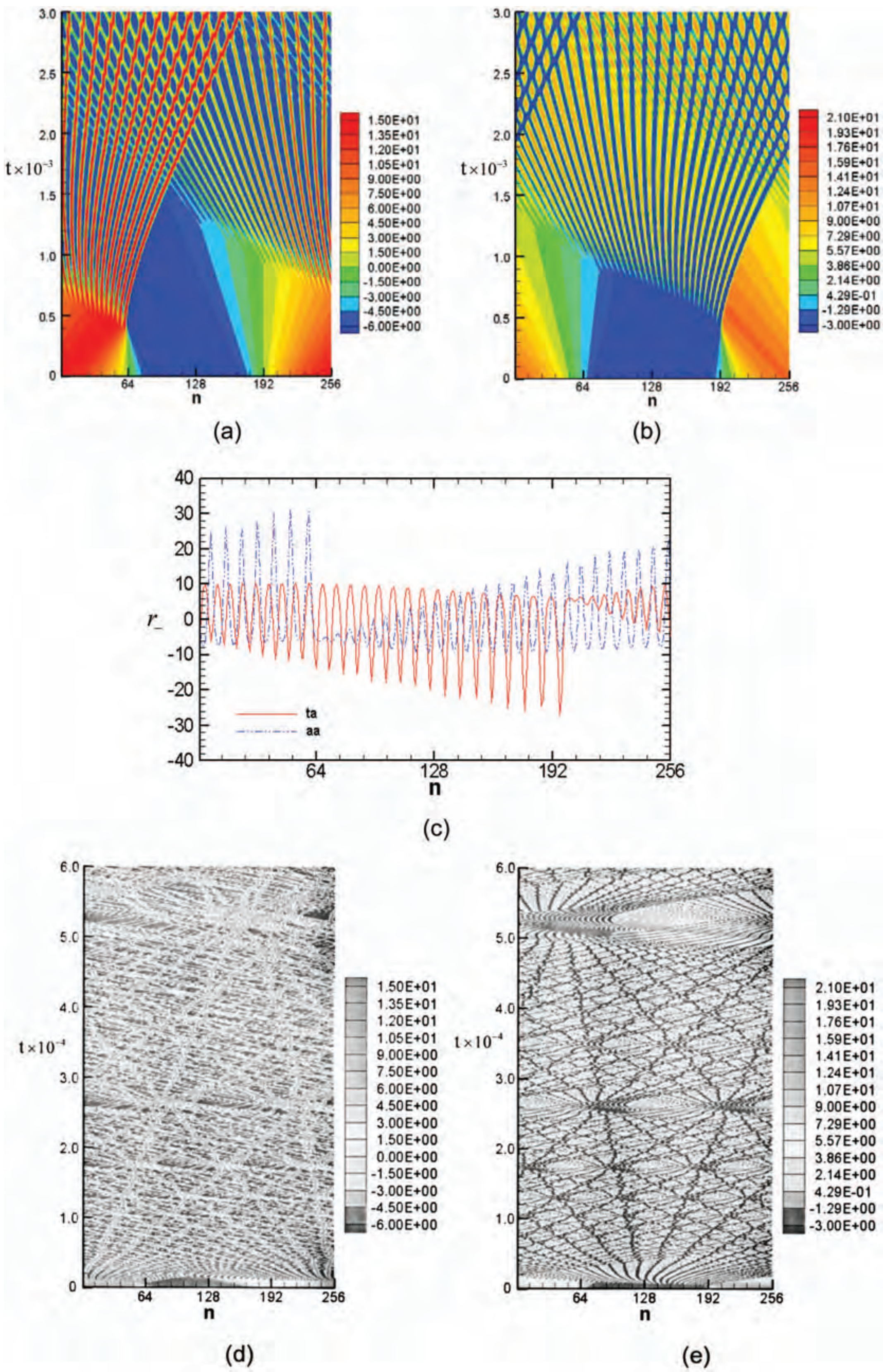

FIG. 5. (Color) Shifted r_- for α and Toda lattice with the acoustic I.C., $N=128$ and $\varepsilon=5.63\times10^{-3}$. (a) s-t diagram for α lattice up to $t=3000$; (b) s-t diagram for Toda lattice up to $t=3000$; (c) at $t^*=1500$, where **ta** is for Toda lattice, and **aa** is for α lattice; (d) s-t diagram for α—lattice up to $t=60\,000$; (e) s-t diagram for Toda lattice up to $t=60\,000$.

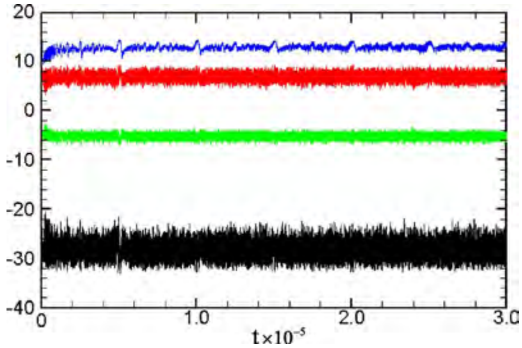

FIG. 6. Toda lattice with the acoustic I.C. ($\varepsilon=5.63\times10^{-3}$). The maximum and minimum of r_- and r_+ vs time for to $t=3\times10^5$. From top to bottom: max(r_-), max(r_+), min(r_+), and min(r_-), respectively.

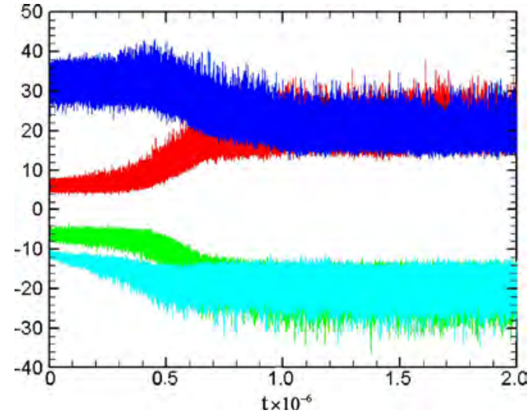

FIG. 7. α lattice with the acoustic I.C. ($\varepsilon=5.63\times10^{-3}$). The maximum and minimum of r_- and r_+ vs time r to $t=2\times10^6$. At early time from top to bottom we have max(r_-), max(r_+), min(r_+), and min(r_-), respectively.

lides with a left going pulse. We say, near-soliton, because the alpha lattice is nonintegrable. A total of 16 pulses emerge. The collisions between large-amplitude near-solitons also exhibit the well-known phase shifts of KdV solitons. The data is for the time interval to just beyond half of a near-recurrence or $\frac{1}{2}T_R=52\,000$. At the arrows at left, one sees the fraction of the near-recurrence times, $\frac{1}{4}T_R$, $\frac{1}{3}T_R$, and $\frac{1}{2}T_R$, times where 4, 5+, and 8 near solitons cluster along the x axis in 4,3, and two groups, respectively.

Another, more quantitative, viewpoint is obtained by plotting versus t, the max and min of r_- and r_+. Note, r_+ is initially zero and its growth is a measure of the coupling of the information flow along the characteristics of the lowest order hyperbolic equation. Figure 3 shows that the initial near sine wave of amplitude 3.15 exhibits a breakdown at $t \sim 1800$ and the leading pulse amplitude grows to 8.2, whereas the mean of min r_- is about 3.1. At t_B the max and min of r_+ grow from *zero* to 0.8. There follows a harmonic type oscillation where max r_+ and min r_+ are 180 deg out of phase. These diagrams on a larger time scale are shown in Fig. 4 and one sees clear evidence of the first near-recurrence at 104 000.

Larger amplitude cases for the alpha and Toda lattices are shown in Figs. 5(a)–5(e).

Note we chose to compare lattices with the same initial average energy, rather than amplitude. Here for both, the energy per unit mass is $\varepsilon=5.63\times10^{-3}$ ($a_{\text{alpha}}=4.33$ and $a_{\text{Toda}}=6.10$).

In Figs. 5(a) and 5(b) (short times for both lattices), we see the emergence for: The alpha lattice of near-solitons (white in B/W and red in color); the Toda lattice of solitons (black in B/W or blue in color). The breakdown time is 400 and one observes the converging characteristics at $n=64$ for alpha and $n=192$ for Toda. [This follows because the Toda

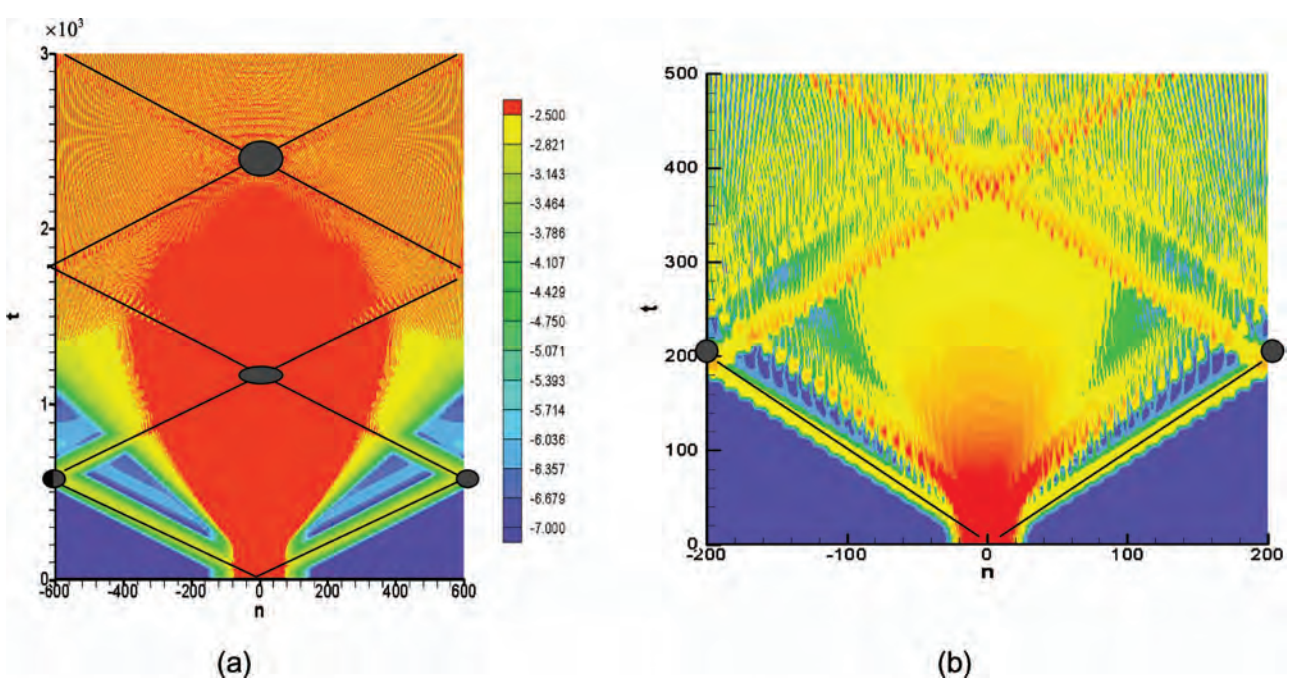

FIG. 8. (Color) Space-time diagrams of the energy of particle j for the α lattice with optical I.C. (a) (log 10-scale) $\eta=0.188$ or $\varepsilon=4.43\times10^{-3}, \alpha=1, \Delta=0.1, N=600$; (b) $\eta=0.326$ or $\varepsilon=1.33\times10^{-2}, \alpha=1, \Delta=0.1, N=200$.

lattice of Eq. (1b) has an α which differs in sign from the FPU α lattice.] A beautiful array of "rays," the soliton trajectories, begins to emerge and one observes thirteen proceeding to the right (i.e., with speeds faster than acoustic) and the remainder proceeding to the left. A slice at $t=1500$ is shown in Fig. 5(c) and one counts 37 maxima for the alpha lattice and 37 minima for the Toda lattice. The *shifted*-$r_{-}(n,t)$ space time diagram shows a cleaner recurrence for Toda than alpha because Toda is integrable and because the dynamics of alpha are becoming chaotic, as discussed below. In *both* cases the first near-recurrence is at $t=5.2\times 10^4$.

We observe a new unusual effect, most clearly in Fig. 5(e), on the *shifted*-$r_{-}(n,t)$ diagram just beyond t_B. This phenomenon is associated with the accumulation of phase shifts due to the *crowding* of near-solitons and packets on a lattice when it is excited by a large amplitude acoustic mode. As Zabusky first noted and has been subsequently shown for the KdV equation, the number of solitons, which emerge from a single long wavelength harmonic, increases with increasing initial amplitude (or average energy). This is evident in the peaks, which emerge from the initial state (red for alpha-lattice and blue for Toda lattice). As these maxima (alpha lattice) grow in amplitude, the strong ones begin to turn to the right. However, when the right going largest amplitude peak interacts with the *mid-amplitude peaks* phase shifts are induced. The *accumulation* of many phase shifts causes several mid-amplitude peaks to move at a reduced average speed. This is most readily seen along a discontinuity in slope of the wave-max trajectory at early times in the range $70<n<186$.

In Fig. 5(d) we compare the s-t of $r_{-}(n,t)$ over the time interval 60 K, including the first recurrence. One sees a clean convergence of rays for Toda and a more chaotic one for alpha. This chaos in convergence of near-solitons is a consequence of the lack of integrability. (In fact, one finds the maximum Lyapounov exponents in Fig. 20 below diverge after the first recurrence.) The curves for max r_{-}, max r_{+}, min r_{+}, min r_{-} for Toda (Fig. 6) and alpha (Fig. 7) are more revealing. The first shows very steady oscillations of nearly constant mean magnitude. However, the mean *magnitudes* are alpha, 34, and Toda, −28. Comparing max r_{-} for Toda shows very recognizable behaviors, including signatures for near recurrence at $t=52$, 104, and 156 K.

Figure 7 shows a much larger variance growth and then as the system becomes chaotic (as discussed below with other diagnostics) both corresponding sets of curves merge, namely the curve of max r_{-} merges with max r_{+} and the curve of min r_{+} merges with min r_{-}. The mean and variance of the curves are both increasing monotonically in magnitude. It would be interesting to relate these differences in the curves to a quantitative diagnostic for integrability.

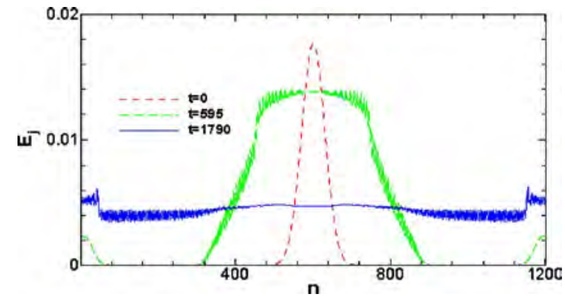

FIG. 9. Energy of particle j for the α lattice with optical I.C. (a) (log 10 scale) $\eta=0.188$ or $\varepsilon=4.43\times 10^{-3}, \alpha=1, \Delta=0.1, N=600$. The curve for $t=0$ is plotted at 0.25 of its true magnitude. Note the spreading between the curves at $t=0$ and $t=595$.

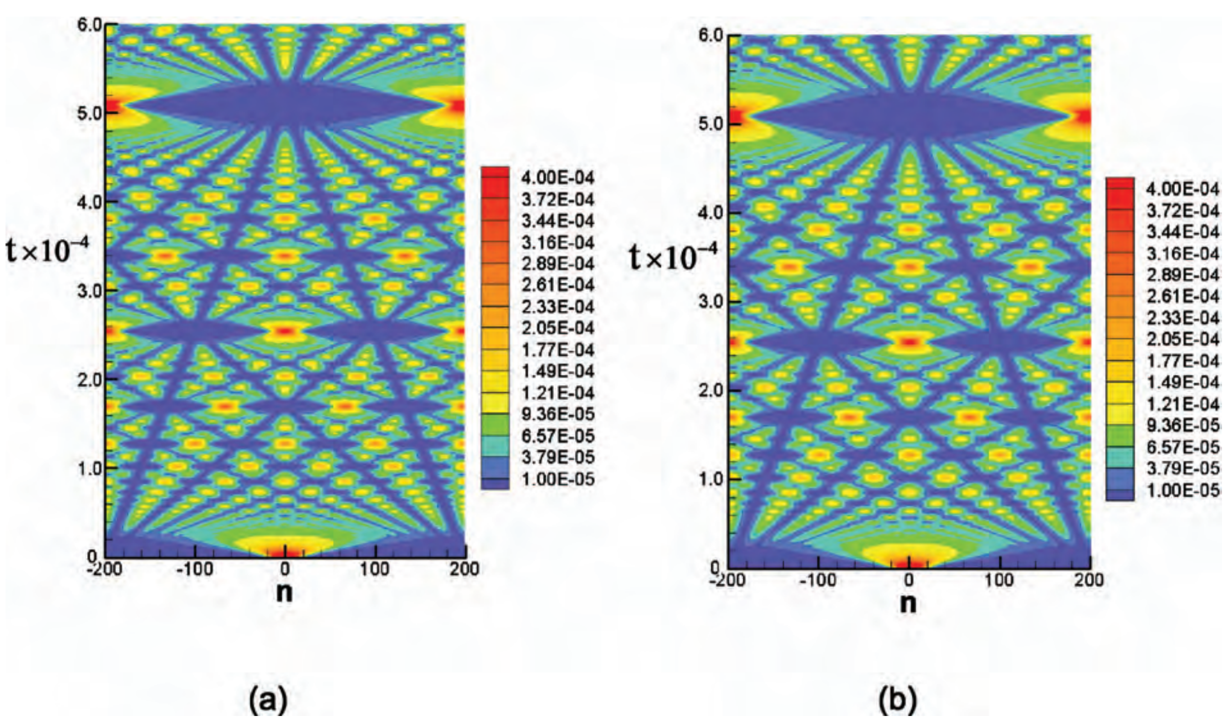

FIG. 10. (Color) Space-time diagrams of the energy of particle j. (a) α lattice with optical I.C. ($\eta=0.02$ or $\varepsilon=5.01\times 10^{-5}, \alpha=1, \Delta=0.1, N=200$); (b) Toda lattice with optical I.C. ($\eta=0.02$ or $\varepsilon=5.01\times 10^{-5}, \alpha=1, \Delta=0.1, N=200$).

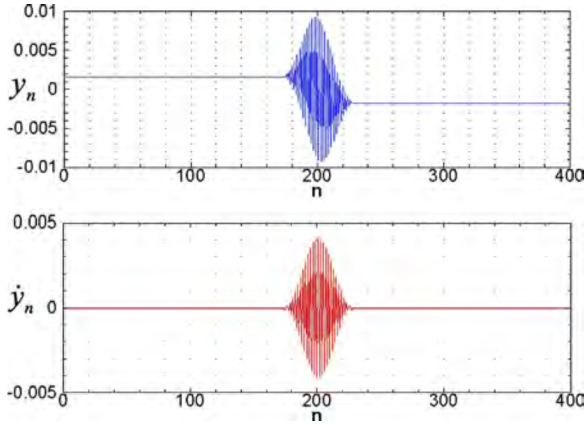

FIG. 11. Localized packet extracted from data corresponding to Fig. 10(a) (α lattice with optical I.C.) ($\eta=0.02$ or $\varepsilon=5.01\times10^{-5}, \alpha=1, \Delta=0.1, N=200$) at the time $t=8510$ where there are four packets on the axis.

OPTICAL EXCITATIONS

Here we set

$$y_j(0) = (-1)^j \eta \exp\left[-\left(\frac{j-N}{\Delta N}\right)^2\right], \quad \dot{y}_j(0) = 0,$$
$$j = 0,1,2,\ldots,2N-1. \tag{14}$$

We present readily available longer time calculations, which exhibit a modulational instability and a new *near recurrence* at small-to-intermediate excitation amplitudes.

In Fig. 8, we show the behavior at short times of the α lattice with the optical I.C. $\eta=0.188$ or $\varepsilon=4.43\times10^{-3}$, $\alpha=1, \Delta=0.1, N=600$ and $\eta=0.326$ or $\varepsilon=1.33\times10^{-2}, \alpha=1, \Delta=0.1, N=200$. We see acoustic pulses emerge symmetrically and strike the boundaries (filled circles) at $t=600$ and $t=200$, respectively. The amplitudes of these Gaussian pulses are in very good agreement with an asymptotical analysis of the Zabusky-Deem equations (1967). The central region (red on the internet) is the spreading optical excitation riding on a smooth gradient (as discussed below). If one compares the rate of increase of the width of the largest (red) region, one sees that the spreading rate increases with the amplitude of the initial excitation. Furthermore, for both excitations the acoustic pulse begins to develop oscillatory-soliton structure at $t>1200$ and $t>200$ in Figs. 8(a) and 8(b), respectively.

This energy is also shown in Fig. 9 [corresponding to Fig. 8(a)] at three times. (Note the curve for $t=0$ is a Gaussian and is plotted at 0.25 scale.)

Figure 10 shows the s-t diagram for this run compared to the Toda lattice, which has an almost identical appearance. In

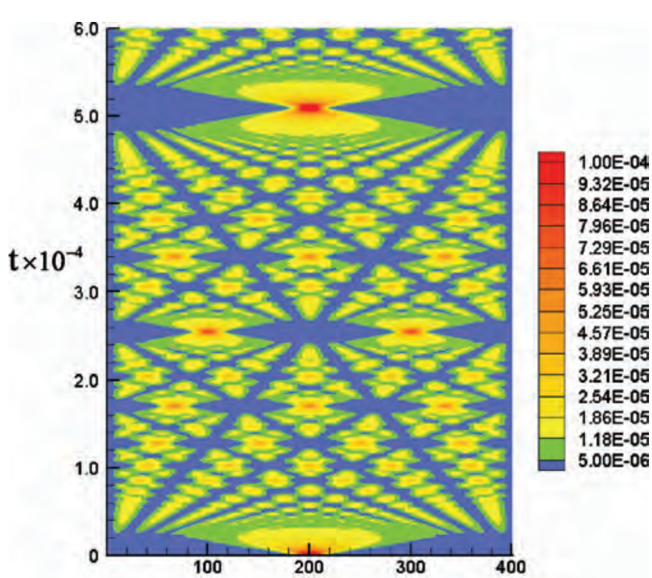

FIG. 12. (Color) Localized packet extracted from data corresponding to Fig. 10(a) (α lattice with optical I.C.) ($\varepsilon=8.36\times10^{-6}, \alpha=1, N=200$).

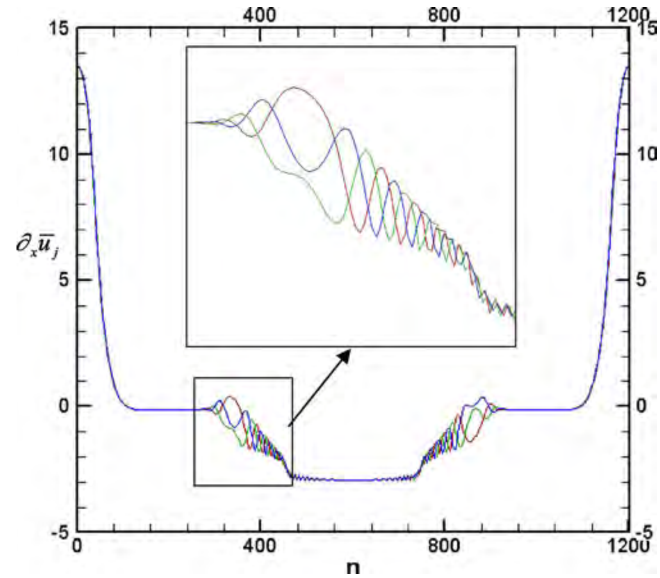

FIG. 13. First derivative filter, Eq. (15), for the FPU α lattice at $t=595$. Note that the acoustical and optical states are single smooth positive and negative curves, respectively. Also, note the symmetrical emergence of slow translating "three-curve" packets.

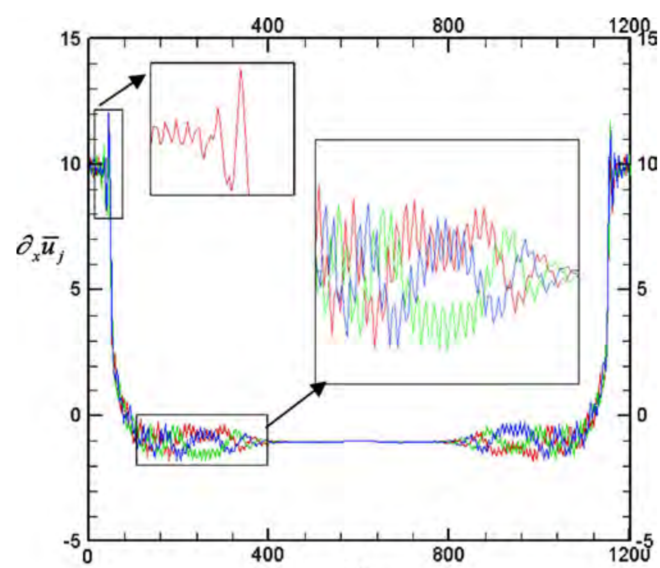

FIG. 14. First derivative filter, Eq. (15), for the FPU α lattice at $t=1790$. Note that the left and right translating acoustical states have evolved while crossing the entire lattice from $t=595$ (Fig. 13) and the symmetrical translating "three-curve" packets have approached closer to the left and right boundaries.

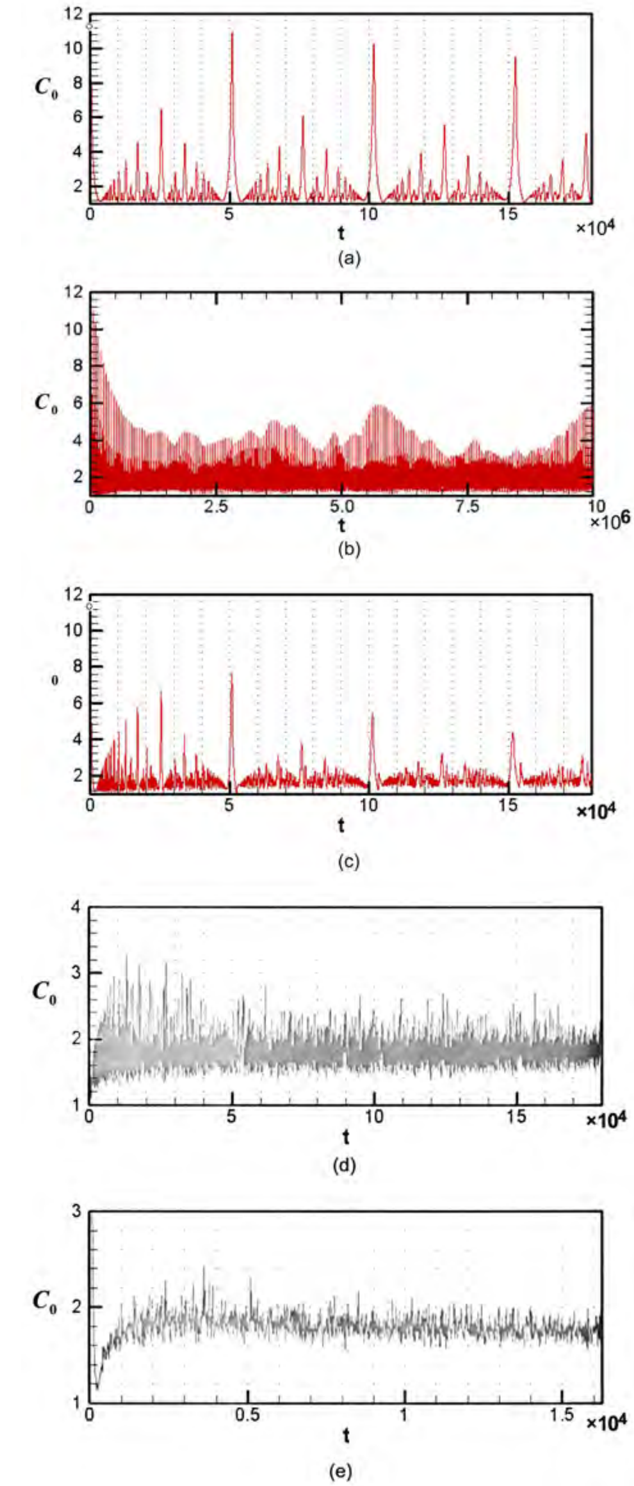

FIG. 15. Localization parameter C_0 for α lattice with optical I.C. (a) $\eta=0.02$ or $\varepsilon=5.01\times10^{-5}$, $\alpha=1$, $\Delta=0.1$, $N=200$; (b) $\eta=0.02$ or $\varepsilon=5.01\times10^{-5}$, $\alpha=1$, $\Delta=0.1$, $N=200$; (c) $\eta=0.06$ or $\varepsilon=4.51\times10^{-4}$, $\alpha=1$, $\Delta=0.1$, $N=200$; (d) $\eta=0.163$ or $\varepsilon=3.33\times10^{-3}$, $\alpha=1$, $\Delta=0.1$, $N=200$; (e) $\eta=0.326$ or $\varepsilon=1.33\times10^{-2}$, $\alpha=1$, $\Delta=0.1$, $N=200$.

both cases a modulational instability arises and localized packets, possibly related to discrete breathers, emerge. These packets interact and focus at $t=51000$. Note, the modulational instability was first analyzed for a pure zone-boundary mode initial excitation by Budinsky and Bountis (1983).

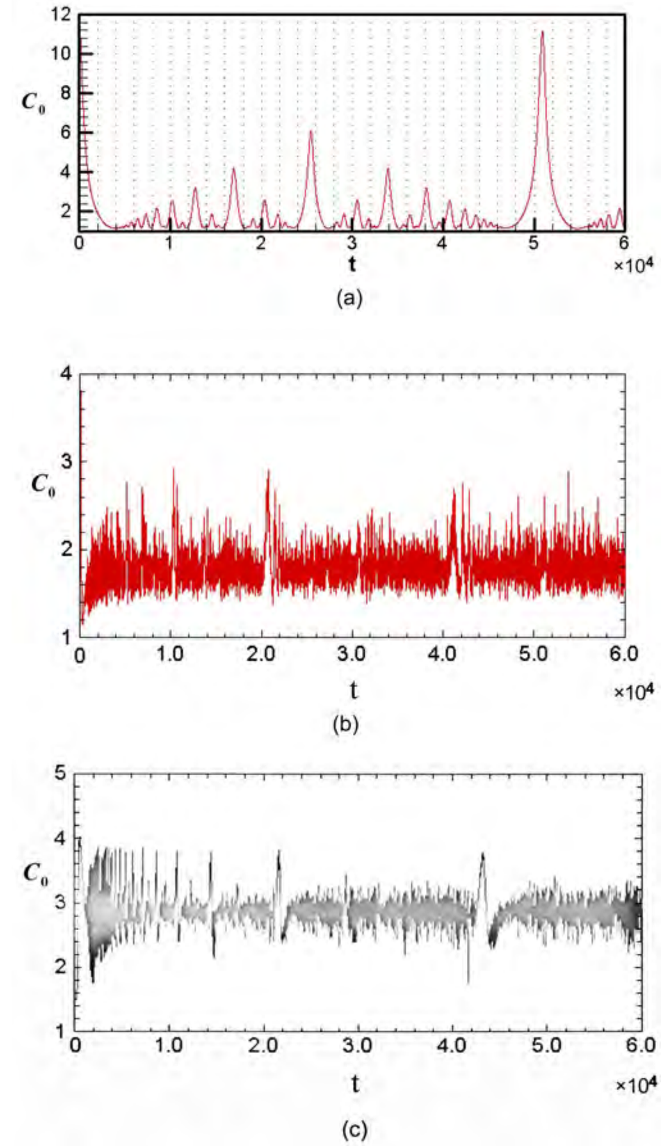

FIG. 16. Localization parameter C_0 for (a) Toda lattice with optical I.C., $\eta=0.02$ or $\varepsilon=5.01\times10^{-5}$, $\alpha=1$, $\Delta=0.1$, $N=200$; (b) Toda lattice with optical I.C., $\eta=0.2885$ or $\varepsilon=1.13\times10^{-2}$, $\alpha=1$, $\Delta=0.1$, $N=128$; (c) Toda lattice with acoustic I.C., $a=6.11$ or $\varepsilon=1.13\times10^{-2}$, $\alpha=1$, $N=128$.

The physical and mathematical behavior of these interacting packets is yet to be understood. As a tentative step we elucidate the evolution of one packet extracted from the data at $t=8150$ and placing it centrally on the lattice, as shown in Fig. 11, where $y_n(8150)$ is above and $\dot{y}_n(8150)$ is below. Note, although the extracted packet is a zone boundary excitation, its displacement is like a *discrete breather* because the values at left and right are of different magnitude. Evolving this state forward with fixed boundary conditions produces the energy space-time diagram in Fig. 12. Remarkably, there is a recurrence. at about the same time, although the focus point is now at the center of the lattice. So these discrete breathers, although unstable, have a remarkable persistence on the periodic and fixed-boundary lattices.

Diagnostic for optical excitations

Although the positive definite energy s-t diagrams and slices present a global view, they do not allow a quantitative

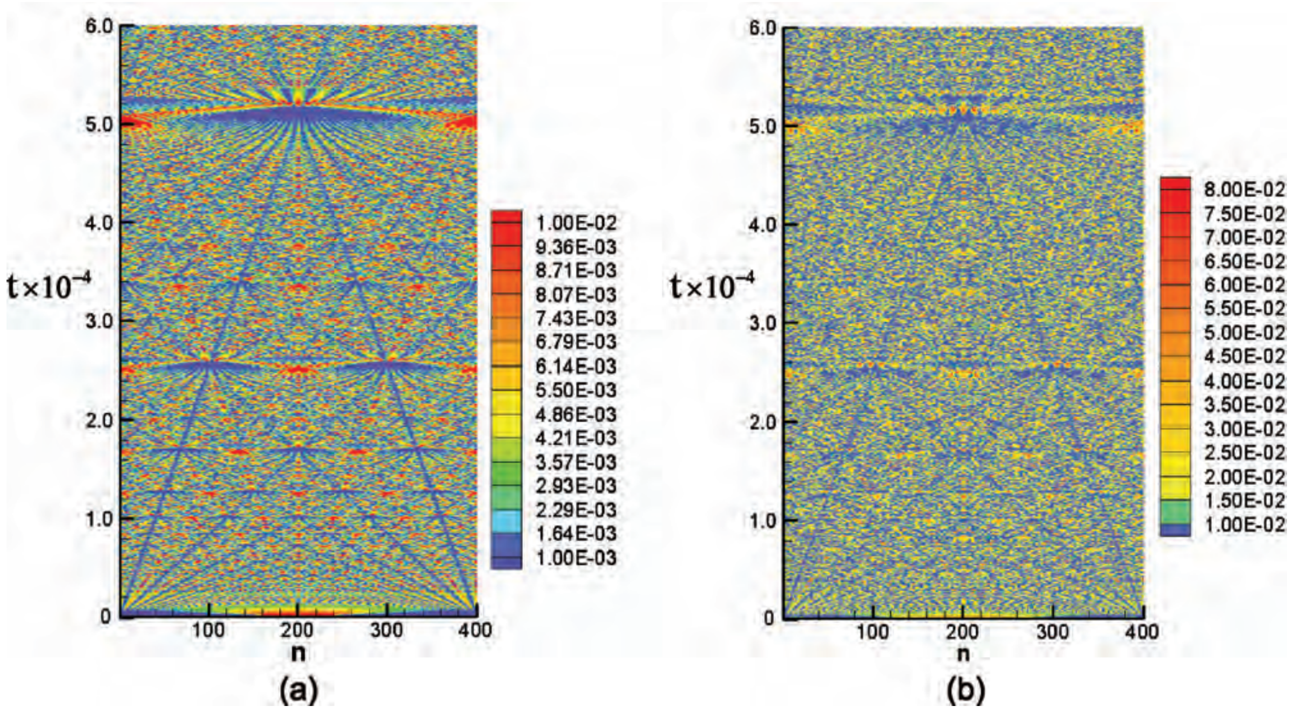

FIG. 17. (Color) Space-time diagrams of the energy of particle j of Toda lattice with optical I.C. (a) $\eta=0.163$ or $\varepsilon=3.41\times10^{-3}$, $\alpha=1$, $\Delta=0.1$, $N=200$; (b) $\eta=0.326$ or $\varepsilon=1.47\times10^{-2}$, $\alpha=1$, $\Delta=0.1$, $N=200$.

appreciation of small but significant effects. We have developed a filter which approximates a spatial derivative and which we designate as

$$\partial_x\bar{u}_j \equiv \tfrac{1}{2}\left\{\delta_x y_j + \tfrac{1}{16}[9(\delta_x y_{j+1} + \delta_x y_{j-1}) - (\delta_x y_{j+3} + \delta_x y_{j-3})]\right\}, \tag{15}$$

where $\delta_x y_j \equiv (y_{j+1} - y_{j-1})/2h$. If the displacements lie along one smooth curve (an acoustic state) then a continuum Taylor series expansion yields

$$\partial_x\bar{u} \to 2y_x + 45\frac{h^4}{5!}y_{xxxxx} + 0(h^6),$$

and if the displacements alternate in sign but each lies along the same smooth curve (an optical state)

$$\partial_x\bar{u} \to +2\frac{h^2}{3!}y_{xxx} - 43\frac{h^4}{5!}y_{xxxxx} + 0(h^6).$$

If the displacement is a mixture of acoustical and optical excitations (e.g., as in our initial condition where the envelopes are Gaussian), then the acoustical signature dominates.

Figure 13 shows $\partial_x\bar{u}$ at $t=595$ and one sees the overlapping acoustical pulses at the boundary and a smooth region $480<n<720$. Also significant is the "three-curve" state radiating symmetrically at $320<n<410$ and $790<n<820$.

Figure 14 shows $\partial_x\bar{u}$ at $t=1790$ and one sees that the overlapping acoustical pulses at the boundary are modulated with emerging solitons and a smooth region that covers the entire lattice. The "three-curve" is at $80<n<400$ and $800<n<1120$.

Diagnostics for chaotic evolutions

We now examine the use of the "*localization parameter*"

$$C_0(t) = N\sum_{j=1}^{2N} E_j^2 \Bigg/ \left(\sum_{j=1}^{2N} E_j\right)^2, \tag{16}$$

to characterize the motion of the α- and Toda lattices, where

$$E_j = \tfrac{1}{2}(\dot{y}_j/\omega_o)^2 + \tfrac{1}{4}[(y_j - y_{j-1})^2 + (y_{j+1} - y_j)^2] + \tfrac{1}{6}\alpha[(y_j - y_{j-1})^3 + (y_{j+1} - y_j)^3] \tag{17}$$

and

$$E_j = \frac{1}{2}\left\{(\dot{y}_j/\omega_o)^2 - \frac{1}{4\alpha^2}[e^{2\alpha(y_j - y_{j+1})} + e^{2\alpha(y_{j-1} - y_j)} - 2\alpha(y_{n-1} - y_{n+1}) - 2]\right\}. \tag{18}$$

If all particles have the same energy (thermalization), $C_0(t)=1.0$. In Figs. 15 and 16, we show results for the α- and Toda lattices. For eta=0.02, Figs. 15(a) and 15(b), we see a regular pattern (reminiscent of the modal energy variation for the FPU acoustic initial excitation). This near recurrent process continues to over 100 near recurrence times! In Figs. 15(c)–15(e), we observe the curve becoming more chaotic and for the largest eta, we see the mean of $C_0\sim1.8$, the lowest of the set (which corresponds to energy equipartition. The C_0 of Fig. 16 (for the Toda lattice) corresponds to Fig. 15(a) and has the same appearance and same recurrence time.

Figures 17(a) and 17(b) show the Toda lattice at high energies. Surprisingly, the near-recurrence is still at t

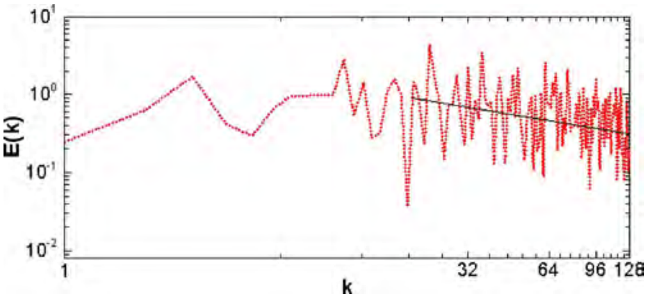

FIG. 18. The spectrum (dashed lines) in log-log scale of Toda lattice with the optical I.C. $\eta=1.304$ or $\varepsilon=9.44\times10^{-1}$, $\alpha=1$, $\Delta=0.1$, $N=128$ at $t=6\times10^4$. The straight solid line is the linear fit of $\log(E(k))$ vs $\log(k)$.

=50 000, but its character is *unusual*. In a narrow time interval we observe a focusing and defocusing that is unlike the first appearance of these structures. There is still much to explain with respect to the interaction of these new coherent structures.

Lyapounov exponents and energy spectra

The nondecreasing variation of the maximum Lyapounov exponent [Casetti *et al.* (1997) and Pettini *et al.* (2005)] and the equidistribution of energy among the Fourier modes have been used to characterize the onset of chaotic or stochastic behavior of a system. A typical spectrum of the Toda lattice and the linear fit with negative slope are shown in Fig. 18.

We now compare these quantities for the alpha and Toda lattice in Fig. 19. Note, at $t\sim800$, after an initial transient, both acoustic and optical evolutions (positive and negative slopes, respectively) have nearly identical slopes. At $t=10^5$ the magnitude of the α-lattice slopes begin to decrease and reach at $t=10^6$ whereas the Toda lattice slopes continue with the same average values.

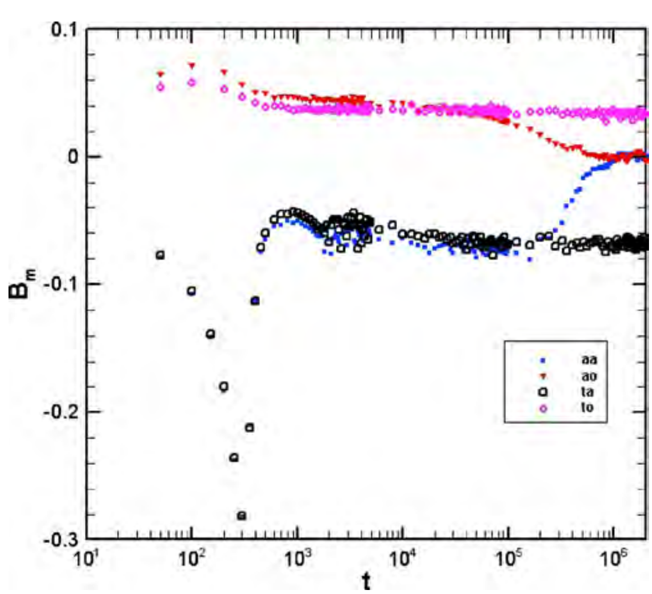

FIG. 19. The variation in slope of the linear fit of $\log_{10}(E(k))$ vs $\log_{10}(k)$, where **aa**—α lattice with acoustic I.C.; **ao**—α lattice with optical I.C.; **ta**—Toda lattice with acoustic I.C.; **to**—Toda lattice with optical I.C.; and $\varepsilon=5.63\times10^{-3}$ for all.

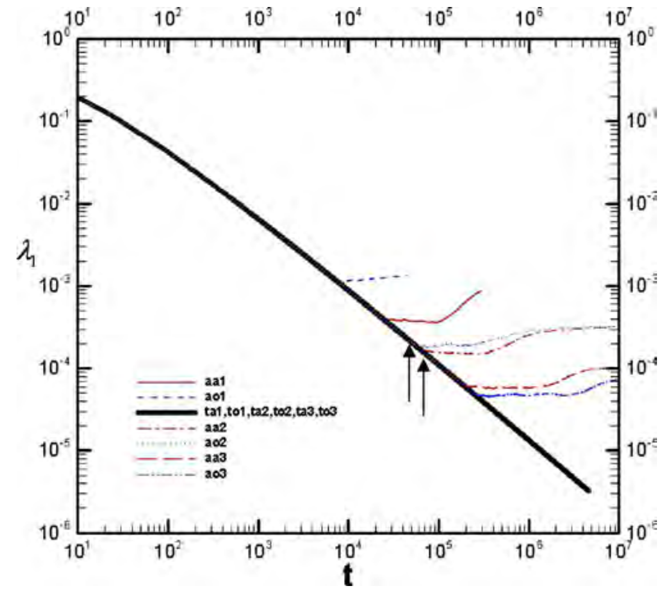

FIG. 20. Lyapounov exponent, where **aa**—α lattice with acoustic I.C.; **ao**—α lattice with optical I.C.; **ta**—Toda lattice with acoustic I.C.; **to**—Toda lattice with optical I.C.; xx1—$\varepsilon=1.12\times10^{-2}$; xx2—$\varepsilon=5.63\times10^{-3}$; xx3—$\varepsilon=2.82\times10^{-3}$. Note: before the α cases diverge from the Toda cases, they share the same curve with the Toda cases.

In Fig. 20, the curves of maximum Lyapounov exponent variation behave like those of the acoustic cases of Casetti *et al.* (1997). For the Toda lattice both acoustic and optical excitations give the *same* curves, independent of the initial amplitude of excitation. For the alpha lattice the larger the initial amplitude the earlier the departure of the curves from the Toda curve.

This departure toward chaos is due to the fact that, in the jargon of nonlinear dynamics, the alpha-lattice has small "islands" of chaotic behavior which the system evolves into at sufficiently long times. It will be interesting in a future study to characterize the size and location of the phase space islands of the alpha-lattice with increasing initial amplitude.

SUMMARY

We have examined the behavior of the one-dimensional alpha-FPU and Toda lattices to optical and acoustic excitations of varying amplitude. We have used the well-known diagnostics: Localization parameter; Lyapounov exponent, slope of linear-fit to linear normal mode energy. Space-time diagrams of the energy per particle and a wave related quantity, the shifted-discretized Riemann invariant have also been shown. The latter is very revealing of soliton and near-soliton properties for the acoustic initial conditions. For the localized optical initial conditions at very early times we have observed, with a special filter, a three-curve state. At later times, we observe coherent structures (packets like discrete breathers) emerge following a modulational instability. These packets interacted and a long time near-recurrence occurred, at a time that was independent of the amplitude of the excitation. This is not related to properties of the acoustic region solitons and the phenomenon has yet to be explained. In all cases all the diagnostic quantifiers, except the localization parameter, showed approach to stochastic or chaotic behaviors for the alpha-lattice at the same time. Thus with the diagnostics shown, there is a clear separation in behaviors at long-time between integrable and nonintegrable systems.

ACKNOWLEDGMENTS

The first author (N.J.Z.) acknowledges valuable conversations with E. G. D. Cohen, L. Friedland, and F. Izrailev and e-mail exchanges with T. Dauxois and B. Rink. T. Dauxois gave us the code with the Yoshida symplectic solver, the Lyapounov diagnostic, and the spectral energy decomposition.

APPENDIX: LARGEST LYAPOUNOV EXPONENT

We use

$$\lambda(t_n) = \frac{1}{t_n}\sum_{n=1}^{N} \ln\left(\frac{\|\xi(t_n)\|}{\|\xi(t_{n-1})\|}\right)$$

where $\xi(t)$ is a tangent, which for our calculations is taken as the particle velocity, $\dot{y}_n$, and $t_n = n\Delta t$ (Δt is some time interval). The computational scheme includes three steps: (1) Start from a random velocity with a given I.C. Make the norm of the velocity vector equal to 1; (2) choose a time interval Δt and apply the above formula to calculate the largest Lyapounov exponent. After the computation of $\lambda(t_n)$, at the end of this time interval, make the norm of the velocity vector equal to 1; (3) repeat the second step until the run terminates.

Berman, G. P., and Izrailev, F. M. (**2005**). "The Fermi-Pasta-Ulam problem: Fifty years of progress," Chaos **15**, 015104.

Budinsky, N., and Bountis, T. (**1983**). "Stability of nonlinear modes and chaotic properties of 1D Fermi-Pasta-Ulam lattices," Physica D **8**, 445–452.

Casetti, L., Cerruti-Sola, M., Pettini, M., and Cohen, E. G. D. (**1997**). "The Fermi-Pasta-Ulam problem revisited: Stochasticity thresholds in nonlinear Hamiltonian systems," Phys. Rev. E **55**, 6566–6574.

Chechin, G. M., Novikova, N. V., and Abramenko, A. A. (**2002**). "Bushes of vibrational modes for Fermi-Pasta-Ulam chains," Physica D **166**, 208–238.

Chechin, G. M., Ryabov, D. S., and Zhukov, K. G. (**2004**). "Stability of low-dimensional bushes of vibrational modes in the Fermi-Pasta-Ulam chains", http://arxiv.org/PS_cache/nlin/pdf/0403/0403040.pdf

Dauxois, T., Khomeriki, R., Piazza, F., and Ruffo, S. (**2005**). "The anti-FPU problem," Chaos **15**, 015110.

Dauxois, T., Ruffo, S., and Torcini, A. (**1997**). "Modulational estimate for the maximal Lyapunov exponent in Fermi-Pasta-Ulam chains," Phys. Rev. E **56**, R6229–R6232.

Dauxois, T., Ruffo, S., and Torcini, A. (**1998**). "Analytical estimation of the maximal Lyapunov exponent in oscillator chains," J. Phys. IV **8**, Pr. 6, 147–156.

Deem, G. S., Zabusky, N. J., and Kruskal, M. D. (**1965**). Formation, propagation, and interaction of solitons in nonlinear dispersive media. This 16 mm film had three parts: (1) Solution of the KdV equation with a sinusoidal initial condition; (2) Solution of the modified-KdV equation with a compressive and rarefactive soliton initial condition; (3) Solution of the nonlinear lattice with a high-frequency ("optical") initial condition. A 16 mm film that was available on free loan from the Bell Telephone Labs film library for over 10 years and will soon be available on the internet at my URL.

Fermi, E., Pasta, J., and Ulam, S. M. (**1955**). "Studies of nonlinear problems," LANL Report, No. 1940; see Fermi's collected works or Stanislaw Ulam *Sets, Numbers, and Universes*, Selected Papers (MIT Press, Cambridge, **1974**).

Izrailev, F. M., and Chirikov, B. V. (**1966**). "Statistical properties of a nonlinear string," in Russian, Sov. Phys. Dokl. **11**, 30 (1965).

Kruskal, M. D., and Zabusky, N. J. (**1964**). "Stroboscopic perturbation procedure for treating a class of nonlinear wave equations," J. Math. Phys. **2**, 231–244.

Pettini, M., Casetti, L., Cerruti-Sola, M., Franzosi, R., and Cohen, E. G. D. (**2005**). "Weak and strong chaos in Fermi-Pasta-Ulam models and beyond," Chaos **15**, 015106.

Rink, B. (**2001**). "Symmetry and resonance in periodic FPU chains," Commun. Math. Phys. **218**, 665–685; see also www.ma.ic.ac.uk/~brink

Rink, B. (private communication, 2005).

Shelepansky, D. (**1997**). "Low energy chaos in the Fermi-Pasta-Ulam problem," Nonlinearity **10**, 1331–38.

Toda, M. (**1967a**). "Vibration of a Chain with Nonlinear Interaction," J. Phys. Soc. Jpn. **22**, 431–436.

Toda, M.. (**1967b**). J. Phys. Soc. Jpn. **23**, 501.

Toda, M. (**1969**). "Mechanics and Statistical Mechanics of Nonlinear Chains," J. Phys. Soc. Jpn. **26**, Suppl. 235–237; Invited paper presented by M. Toda at the International Conference on Statistical Mechanics, Kyoto, Japan, September, 1968.

Toda, M. (**1989**). *Theory of Nonlinear lattices*, 2nd ed. (Springer, Berlin).

Tuck, J. L., and Menzel, M. T. (**1972**). "The superperiod of the nonlinear weighted string (FPU) problem," Adv. Math. **9**, 399.

Yoshida, H. (**1990**). "Construction of higher order symplectic integrators," Phys. Lett. A **150**, no. 5–7, 262–268.

Zabusky, N. J., and Kruskal, M. D. (**1965**). "Interaction of solitons in a collisionless plasma and the recurrence of initial states," Phys. Rev. Lett. **15**, 240–243.

Zabusky, N. J. (**1962**). "Exact solution for the vibrations of a nonlinear continuous model string," J. Math. Phys. **5**, 497–499.

Zabusky, N. J. (**1967**). "A synergetic approach to problems of nonlinear dispersive wave propagation and interaction," in Proceedings of the Symposium Nonlinear Partial Differential Equations, edited by W. Ames (University of Delaware, Newark, Delaware, published by Academic Press, New York, 1967). This invited paper was presented in 1965.

Zabusky, N. J. (**1969**). "Nonlinear lattice dynamics and energy sharing," J. Phys. Soc. Jpn. **26**, Suppl., p. 196; Invited paper presented at the International Conference on Statistical Mechanics, Kyoto, Japan, September, 1968.

Zabusky, N. J. (**1981**). "Computational synergetics and mathematical innovation," J. Comput. Phys. **43**, 195–249.

Zabusky, N. J. (**2005**). "Fermi-Pasta-Ulam, solitons and the fabric of nonlinear and computational science: History, synergetics and visiometrics," Chaos **15**, 015102.

Zabusky, N. J., and Deem, G. S. (**1967**). "Dynamics of nonlinear lattices I, localized optical excitations, acoustic radiation and strong nonlinear behavior," J. Comput. Phys. **2**, 126–153.